TU Delft

Delft University of Technology

Real-time photoacoustic assessment of radiofrequency ablation lesion formation in the left atrium

Iskander-Rizk, Sophinese; Kruizinga, Pieter; Beurskens, Robert; Springeling, Geert; Mastik, Frits; de Groot, Natasja M.S.; Knops, Paul; van der Steen, Antonius F.W.; van Soest, Gijs

DOI
10.1016/j.pacs.2019.100150

Publication date
2019

Document Version
Final published version

Published in
Photoacoustics

Citation (APA)
Iskander-Rizk, S., Kruizinga, P., Beurskens, R., Springeling, G., Mastik, F., de Groot, N. M. S., Knops, P., van der Steen, A. F. W., & van Soest, G. (2019). Real-time photoacoustic assessment of radiofrequency ablation lesion formation in the left atrium. *Photoacoustics*, *16*, Article 100150. https://doi.org/10.1016/j.pacs.2019.100150

Important note
To cite this publication, please use the final published version (if applicable).
Please check the document version above.

Copyright
Other than for strictly personal use, it is not permitted to download, forward or distribute the text or part of it, without the consent of the author(s) and/or copyright holder(s), unless the work is under an open content license such as Creative Commons.

Takedown policy
Please contact us and provide details if you believe this document breaches copyrights.
We will remove access to the work immediately and investigate your claim.

This work is downloaded from Delft University of Technology.
For technical reasons the number of authors shown on this cover page is limited to a maximum of 10.

Photoacoustics 16 (2019) 100150

Contents lists available at ScienceDirect

Photoacoustics

journal homepage: www.elsevier.com/locate/pacs

Real-time photoacoustic assessment of radiofrequency ablation lesion formation in the left atrium

Sophinese Iskander-Rizk[a,*], Pieter Kruizinga[b], Robert Beurskens[a], Geert Springeling[c], Frits Mastik[a], Natasja M.S. de Groot[a], Paul Knops[a], Antonius F.W. van der Steen[a,d], Gijs van Soest[a]

[a] Department of Cardiology, Erasmus MC, University Medical Center Rotterdam, the Netherlands
[b] Department of Neuroscience, Erasmus MC, University Medical Center Rotterdam, the Netherlands
[c] Department of Experimental Medical Instruments, Erasmus MC, University Medical Center Rotterdam, the Netherlands
[d] Department of Imaging Physics, Faculty of Applied Sciences, Delft University of Technology, Delft, the Netherlands

ARTICLE INFO

Keywords:
Photoacoustic imaging
Photoacoustic-enabled RF ablation catheter
Lesion monitoring
Atrial fibrillation
RF ablation

ABSTRACT

In interventional electrophysiology, catheter-based radiofrequency (RF) ablation procedures restore cardiac heart rhythm by interrupting aberrant conduction paths. Real-time feedback on lesion formation and post-treatment lesion assessment could overcome procedural challenges related to ablation of underlying structures and lesion gaps. This study aims to evaluate real-time visualization of lesion progression and continuity during intra-atrial ablation with photoacoustic (PA) imaging, using clinically deployable technology. A PA-enabled RF ablation catheter was used to ablate and illuminate porcine left atrium, both excised and intact in a passive beating heart ex-vivo, for photoacoustic signal generation. PA signals were received with an intracardiac echography catheter. Using the ratio of PA images acquired with excitation wavelengths of 790 nm and 930 nm, ablation lesions were successfully imaged through circulating saline and/or blood, and lesion gaps were identified in real-time. PA-based assessment of RF-ablation lesions was successful in a realistic preclinical model of atrial intervention.

1. Introduction

Atrial fibrillation (AF) is the most common and most persistent arrhythmia with high morbidity and mortality rates [1]. AF is associated with an increased probability of stroke, heart failure and hospitalization. Radiofrequency (RF) ablation is one of the potential curative treatments of AF. In RF ablation procedures, a catheter is positioned in the left atrium to isolate the pulmonary veins (PV) and create additional lesions in areas with fractionated potentials as needed, guided by electroanatomical maps. During these long-lasting procedures, tissue is ablated (rendered nonconductive) with RF energy to isolate the PV, while being cautious not to ablate underlying structures such as the esophagus. The procedural success rate of AF ablation is approximately 60–80 % when accounting for redo ablations [2–4]. This low success rate is mostly attributed to PV reconnection or the presence of an extensive arrhythmogenic substrate outside the PV [5–7]. Gaps in the lesion trace as well as the inability to discern edema from tissue necrosis may result in arrhythmia recurrence [5,8]. Catheter positions, contact force and local electrograms can be measured and visualized, but treatment delivery and lesion extent are estimated based on a combination of thermodynamic- and biophysics-based models and heuristics for the different atrial sites [9,10] without regard for anatomical variations among patients. Development of a tool that provides direct lesion visualization, assessment and monitoring could potentially increase the success rate of this procedure [5,11].

Thus far, Magnetic Resonance Imaging (MRI) and ultrasound elastography were the only two imaging modalities shown to assess RF ablation lesions in humans. However, both face challenges in monitoring lesion formation during RF energy delivery due to device compatibility, temporal resolution and motion artefacts caused by an asynchrony of acquisitions in an irregular heart rhythm [12,13]. Ultrasound imaging studies [14,15] showed promising results in monitoring RF ablation lesions in animal models but the small field of view of the imaging catheters that were used limits the assessment of the lesion as a whole. In addition, the image features characterizing ablation lesions were neither consistent between studies [16] nor persistent in ex-vivo evaluation setups [17]; a necessary feature for post-ablation lesion continuity assessment. Optical methods, such as near infrared spectroscopy (NIRS), or polarization sensitive-/ optical coherence tomography (PS-/OCT), were also considered for the problem of lesion

* Corresponding author at: Department of Biomedical Engineering, Erasmus Medical Center, Ee-2322, Wytemaweg 80, 3015 CN, Rotterdam, the Netherlands.
E-mail address: s.iskander-rizk@erasmusmc.nl (S. Iskander-Rizk).

https://doi.org/10.1016/j.pacs.2019.100150
Received 1 June 2019; Received in revised form 24 October 2019; Accepted 13 November 2019
Available online 30 November 2019
2213-5979/ © 2019 The Author(s). Published by Elsevier GmbH. This is an open access article under the CC BY-NC-ND license (http://creativecommons.org/licenses/BY-NC-ND/4.0/).

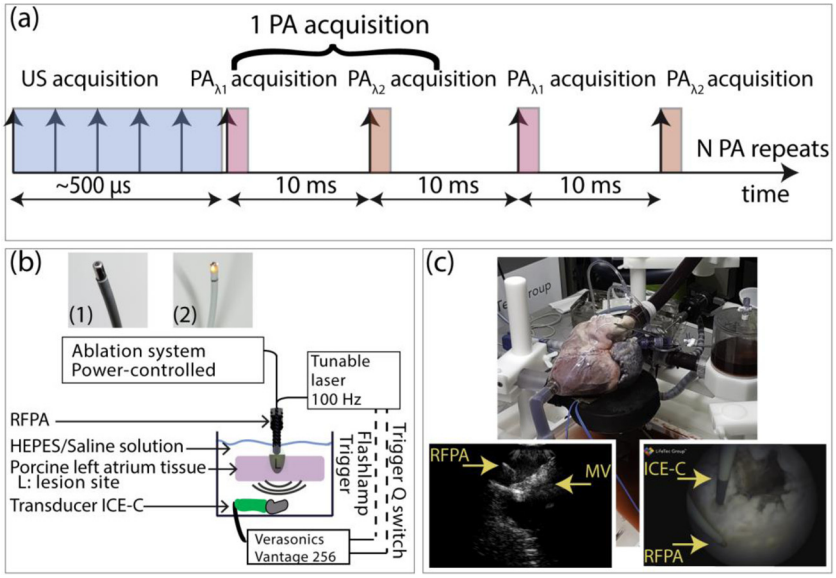

Fig. 1. Methodology. (a) An imaging frame consists of 5 ultrasound acquisitions and N photoacoustic acquisitions composed of acquisitions at λ1 = 790 nm and λ2 = 930 nm. The shaded area represents the signal acquisition time. The setup comprises an ultrasound research system, a tunable laser and an ablation system. (b) Excised porcine tissue is imaged in transmission mode photoacoustic with the ablation catheter on the endocardium side. Insert (1) is a photograph of the single fiber catheter RFPA catheter prototype and insert (2) of the three-fiber RFPA catheter. (c) Photo of the beating heart setup with the ablation indifferent electrodes positioned under the heart and the circulating fluid is blood. Real-time US/PA monitoring and endoscopy were available. The bottom of the figure shows snapshots of both the endoscope monitoring screen looking down at the mitral valve (bottom right) and of the intracardiac echography monitoring screen (bottom left). Intracardiac echo catheter: ICE-C, PA-enabled RF ablation catheter: RFPA, Mitral valve: MV.

monitoring [18–21]. However, NIRS imaging contrast relies heavily on optical modelling, which is sensitive to device and tissue geometry. NIRS is therefore likely to be affected by variations in tissue thickness and by the sampling catheter orientation in the highly mobile environment of a beating heart. Spectroscopic approaches are though currently being researched towards solving this challenge [22,23]. An OCT based solution to monitoring ablation lesion formation in real-time looks very promising, considering it provides the highest resolution of all considered modalities. PS-/OCT-enabled ablation catheter prototypes were demonstrated [20,21] to simultaneously ablate and image lesion extent using both tissue birefringence signal as well as tissue scattering changes. However, OCT methods have yet to be demonstrated on atrial tissue and are more limited than photoacoustic methods in imaging depth.To this day, no imaging technology provides real-time, complete and/or reliable means for AF treatment monitoring and evaluation, either lacking feedback during energy delivery, or capacity to assess lesion continuity and quality post energy delivery.

Photoacoustic (PA) imaging contrast relies on tissue optical absorption. Photoacoustic imaging requires an illumination source and an ultrasound transducer to detect acoustic waves generated by light absorption. Ablated tissue is optically different from untreated tissue. White-light video endoscopy, used to guide laser-ablation procedures, confirms that this contrast also exists in vivo. Previous studies showed that PA imaging can monitor lesion progression during RF delivery in ex-vivo porcine myocardium [24–26]. We have previously characterized ablated and non-ablated porcine atrial tissue and found PA spectroscopic differences between the two types, likely related to changes in hemichrome, methmyoglobin and protein denaturalization contents. Spectroscopic based imaging was reliably reduced to a dual wavelength PA imaging scheme, which was shown to robustly assess lesions in porcine atrial tissue with 97 % diagnostic accuracy [25]. From an instrumentation perspective, ablation catheters combining the delivery of both radiofrequency current for ablation and pulsed laser light for simultaneous photoacoustic imaging were previously demonstrated to enable ablation lesion monitoring [27,28]. We take a next step in the clinical translation of this concept with intracardiac ablation imaging. We also use an actual ICE catheter for signal collection, introducing its characteristic small aperture and modest sensitivity.

This study aimed to assess lesion progression and continuity during intra-atrial ablation with photoacoustic imaging in real-time, using technology that is compatible with clinical deployment. Porcine atrial tissues ex vivo were used, both excised and in a beating heart setup, in saline and in blood. These experiments demonstrate the potential of PA imaging feedback of RF-induced tissue changes for energy delivery titration as well as for evaluation of lesion transmurality and identification of lesion gaps, which are important parameters for successful, permanent and safe ectopic source isolation.

2. Methods

2.1. Imaging system

The imaging system uses technology that is commonly found in interventional electrophysiology clinics. An ICE catheter (3.1 mm outer diameter, 2.45 mm at the tip, 60/64 connected channels, 6.5 MHz, ViewFlex, St Jude Medical, Saint Paul, Minnesota) was connected to a research ultrasound system (Verasonics Vantage256, Kirkland, Washington) for signal digitization, processing and display. A medical RF generator (EPT1000XP APM system, Boston Scientific, Marlborough, Massachusetts) delivered energy to an ablation catheter (Blazer, EPT9620K2, Boston Scientific, Marlborough, Massachusetts), modified to deliver laser light (RFPA catheter). The RFPA catheter used for most of the experiments was of 2.4 mm (7 F) outer diameter and fitted one 400 µm core diameter, NA = 0.39 multi-mode optical fiber (FT400EMT, Thorlabs, Newton, NJ) through the flushing channel [27]. An alternative design, used in the blood-filled heart, comprised three 200 µm fibers (FP200ERT, Thorlabs, Newton, NJ) placed around the ablation tip; the catheter outer diameter was of 2.4 mm ending in an ablation tip electrode of 1.8 mm (Fig. 1b2). PA imaging performance of both catheters was previously found to be similar [27]. The RFPA catheter was also connected to a tunable, 100 Hz pulsed laser (660 – 2400 nm, 6 ns pulse width, Spitlight EVO-OPO, Innolas, Krailling, Germany). This way, the RFPA catheter can deliver excitation light directly at the ablation site, enabling simultaneous ablation and PA imaging of cardiac tissue.

2.2. Image acquisition and processing

The imaging sequence consisted of five ultrasound pulse-echo (diverging wave) acquisitions, followed by *N* paired PA acquisitions at 790 and 930 nm (Fig. 1a). Signal digitization, filtering and image reconstruction was performed using the Verasonics software. Ultrasound time gain compensation (TGC) was adjusted as needed during the imaging based on real-time feedback, while the PA TGC was fixed to a maximum and not controllable during the acquisition. PA images were averaged (*N* times) and corrected for laser fluence fluctuations. Single

wavelength images are labeled by their excitation wavelength λ (I_λ). N is minimized and optimized to achieve adequate signal-to-noise ratio (SNR), which depends on the laser pulse energy and RFPA catheter alignment with the ICE catheter imaging plane. The relative excitation pulse energy was inferred from the signal originating at the catheter tip.

Dual wavelength PA imaging (2λPA), defined as the ratio of I_{790} to I_{930}, can identify and delineate ablation lesions [25]. To monitor lesion progression and compensate for the effects of cardiac motion and laser optical output variability, 2λPA images were further processed. Since the 2λPA image SNR depends on the initial image quality, I_{790} and I_{930} frames of sufficient SNR were smoothed along the frames using a 1st order Savitzky–Golay filter of length equal to the number of frames in one heartbeat. For the static experiments, we set the filter length to 5. Moreover, 2λPA is a ratio thresholding method, thus, to remove any random additive noise we subtract the mean (μ represents the mean operation) from each image before taking the ratio:

$$S_R = \frac{I_{790} - \mu(I_{790})}{I_{930} - \mu(I_{930})} \quad (1)$$

Any random spurious noise will be enhanced by the division operation, which is suppressed by a moving average filter based on the previous 3 frames: $\frac{1}{3}\sum_{i-2}^{i} S_R$ to compute the final 2λPA image. 2λPA imaging, at the selected wavelengths, theoretically ensures that non-ablated tissue of varying tissue oxygenation levels – as well as blood – display $S_R < 1$ while lesion areas are characterized by $S_R > 1$ [25]. 2λPA imaging also ensures that signal increase solely reflects tissue changes, not temperature variations [29].

We measured that 1 mJ of optical input can penetrate up to 8 mm of porcine atrial tissue at the chosen wavelengths. However, with laser pulse-to-pulse energy decrements, penetration depth can be reduced. 2λPA imaging depth cannot exceed the smallest probed depth by any of the I_λ images used. To only display information with sufficient fidelity, the final 2λPA image is masked based on the minimum SNR of either PA image.

Finally, by compounding 2λPA images for different RFPA catheter positions, registered using echo information, continuity of lesions post ablation is evaluated. Criteria for frame selection are (1) SNR ≥ 10 dB and (2) high correlation between the frames on ultrasound. Final, compounded images are binary images composed of multiple 2λPA frames processed such that pixels above a threshold of 1 are set to red and the rest to NaN.

2.3. Ablation of excised cardiac tissue

Fresh (0 − 24 h after slaughter) porcine atrial tissue from the local butcher was mounted with wires on a holder, and submerged in phosphate-buffered saline (PBS) [25]. The ICE catheter was positioned on the epicardial side and the RFPA catheter on the endocardial side (Fig. 1b). Four laser pulses were averaged to form a single photoacoustic image ($N = 4$), yielding a frame rate of 12.5 Hz. The average pulse energy delivered at the catheter tip was ~1 mJ at 790 nm and ~0.6 mJ at 930 nm. The ablation system used did not have irrigation capability. Ablation was performed in power-controlled mode (25 W for 25 s), since temperature feedback was not available from the modified catheter. Four ablation lesions were formed and imaged in real-time. We also assessed the continuity of the lesions by moving and flexing the RFPA catheter around the lesions made, aiming to illuminate and generate signals from the entire treated volume (as opposed to at lesion sites only). During the manipulation, we did not move the receiving ICE catheter. The result is thus an evaluation of the lesion continuity within the imaging 2D plane probed by the ICE.

2.4. Ablation in a passive beating heart

A porcine heart was mounted in a circulation system (Cardiac Biosimulator, LifeTec Group, Eindhoven, Netherlands), filled with 5 liters of fluid (saline or heparinized blood). The fluid flowed from the aorta and drained through an opening made in the apex of the left ventricle (Fig. 1c); other cavities were filled through hydrostatic pressure. A pulsatile pump, set to 1 Hz, created a fluid flow of 4.5 L/min. This setup is a representative model for cardiac motion and is frequently used in the training of catheter-based cardiac interventions [30]. We inserted the RFPA and ICE catheters through the jointly tied PV into the left atrium. When working in saline, the video endoscope, positioned in the PV, visualizes the catheters and the sites where we applied RF energy (10 − 30 W, 35 s) (Fig. 1c). I_λ were not averaged ($N = 1$), enabling an effective excitation frame rate of 50 Hz. Due to memory management limitations in our ultrasound system, the saving frame rate varied and was restricted to 6 Hz maximum.

In saline, we monitored a series of ablation lesions (without catheter irrigation) on the mitral annulus and nearby tissue, documenting them on video. Blood precludes the use of the video endoscope. Thus, prior to flushing the heart with heparinized blood, we positioned the catheters under endoscopic guidance, such that the ICE catheter images capture the RFPA catheter. In blood, we monitored the formation of one lesion (30 W, 30 s). After imaging, the heart was cut open, washed and its inner surface evaluated for lesions. With the aid of the endoscopy videos, all lesions could be related to the imaging acquisitions. We cut through the lesions to examine depth and extent, documenting them in photographs.

3. Results

3.1. RF ablation monitoring in a static setup

We monitored lesion formation in a static setup with the 2λPA imaging scheme. Fig. 2 documents the monitoring of a lesion made in this specimen. We set timepoint t = 0 to represent the beginning of ablation. Comparison of I_λ frames (Fig. 2b) to 2λPA (Fig. 2a) frames at the beginning of ablation shows robustness of the latter in eliminating signals from the catheter tip. The final 2λPA image clearly delineates the lesion, matching the photograph in Fig. 2d. 2λPA imaging is less affected by RF interference artefacts. These are prominent in I_λ, depending on the image SNR. 2λPA monitoring of the lesion formation depicted by Fig. 2 is included as Movie 1. Intermittent glitches of signals occur when the RFPA catheter relocates, or when it is deforming the tissue, as a result of $N = 4$ frame averaging. The formed lesion seemed superficial which was confirmed by cutting through the tissue at the lesion site, Fig. 2d. A clear advantage of 2λPA imaging over single wavelength PA (I_λ) imaging (Fig. 2) is a simple and intuitive binary representation of the presence/absence of lesion allowing easy lesion progression visualization.

In total, formation of four lesions was successfully monitored in this manner, Fig. 3. Each lesion is labeled with a number. Ablation lesion continuity is key to procedural success. Point source light delivery from the RFPA catheter limits the imaging field of view to the illuminated area. To obtain an overall view of all lesions made, we moved the RFPA catheter to illuminate all the treated region and recorded the signals. Compounded acquisitions formed one final image revealing lesion continuity along the ICE imaging plane Fig. 3a). Gaps were identified between lesions 1 and 2 and between 3 and 4, while 2 and 3 are overlapping.

3.2. RF ablation monitoring in a beating heart ex vivo in saline

In a beating heart filled with circulating saline, we applied RF energy for various durations and power settings. We monitored the formation of four ablation lesions. Fig. 4 shows a lesion being created (using 28 W for 35 s). Both the RFPA catheter and ICE catheter were positioned around the mitral valve as shown in Fig. 4,e. Fig. 4a depicts 2λPA images before, after and during ablation and Fig. 4b their

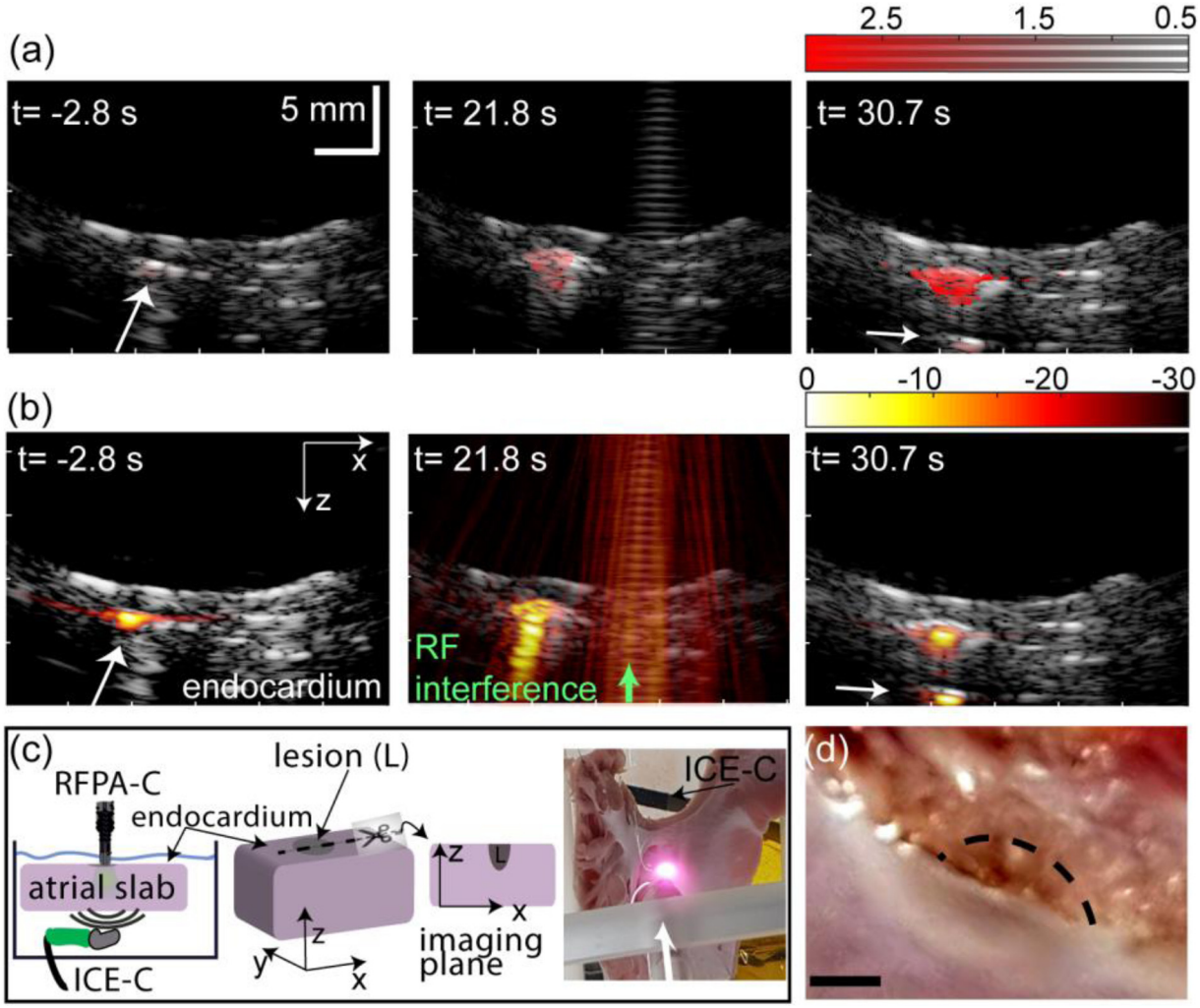

Fig. 2. Ablation monitoring of excised left atrium. (a) 2λPA images before, during and after ablation, available as Movie 1. The 2λPA signal is encoded as opacity of the red overlay on the ultrasound image. (b) Corresponding I_{790} images. Ultrasound (US) image is in grayscale. Photoacoustic image is in red-yellow-white scale. (c) Photograph of the setup. (d) Photograph of lesion made, dashed line delineates lesion extent. Scale bar represents 2 mm. White arrows indicate ablation (RFPA-C) catheter location.

equivalent I_{790} frames. As in the static setup, 2λPA imaging enables lesion formation visualization, while it remains challenging to distinguish lesions from untreated tissue sites and from the RFPA catheter tip on I_{λ} images. Movie 2 documents the process of ablation, with a final lesion signal reflecting its true size (Fig. 4c). Fig. 4d is a frame from the endoscope used to monitor and guide the procedure, illustrating the tissue surface discoloration after removing the catheter from the ablation site. A small deflection/crater (cyan arrows Fig. 4) at the tissue surface appeared where the ablation was performed. This further confirms that ultrasound, PA and endoscopy video data all had the ablation site in view.

Lesion continuity and gap sizing is evaluated in the beating heart setting by serially ablating two sites in one ICE scene. After monitoring the formation of yet another lesion, we dragged the RFPA catheter to the closest (previously ablated) lesion site within the ICE catheter field of view, guided by the video endoscope. Movie 3 shows the monitoring of the lesion formation as well as the movement of the catheter to the closest lesion site, where the endoscope frame rate is matched to that of our acquisition scheme. Fig. 5a,b show post-ablation 2λPA images and their corresponding endoscopy frames, and lesions as photographed in tissue. A compound image, based on 2λPA image pixels of $S_R > 1$, enables lesions respective localization and allows sizing of the gap in between (Fig. 5c). Cardiac motion required correlating ICE imaging frames before compounding. We successfully identified ablation gaps in the challenging setup of a beating heart with a 2D ultrasound field of view.

To qualitatively assess the specificity of the PA signal for ablated tissue, we evaluated a control case of low energy delivery (10 W, 35 s). Endoscopic images showed no tissue surface discoloration suggesting no tissue ablation occurred; this was later confirmed by post-experimental tissue examination. Fig. 6a documents the energy delivery process with 2λPA imaging, confirming the absence of lesion formation, also available as Movie 4. No persistent lesion-like signal is observed. Incidental glitches may result from imperfect laser pulse energy fluctuation correction since $N = 1$. Single wavelength PA (I_{λ}) images (Fig. 6b), on the other hand, hardly discriminate the presence or absence of lesion. Fig. 6c,d illustrate catheter positions relating the tissue structures observed on ultrasound.

3.3. Visualization of lesion formation in blood

Blood has a high optical absorption coefficient and could potentially interfere with PA imaging, by showing as a positive signal, or by strongly attenuating the light reaching the tissue. We designed the presented imaging technology for compatibility with blood by placing the light source in contact with the tissue. We tested imaging

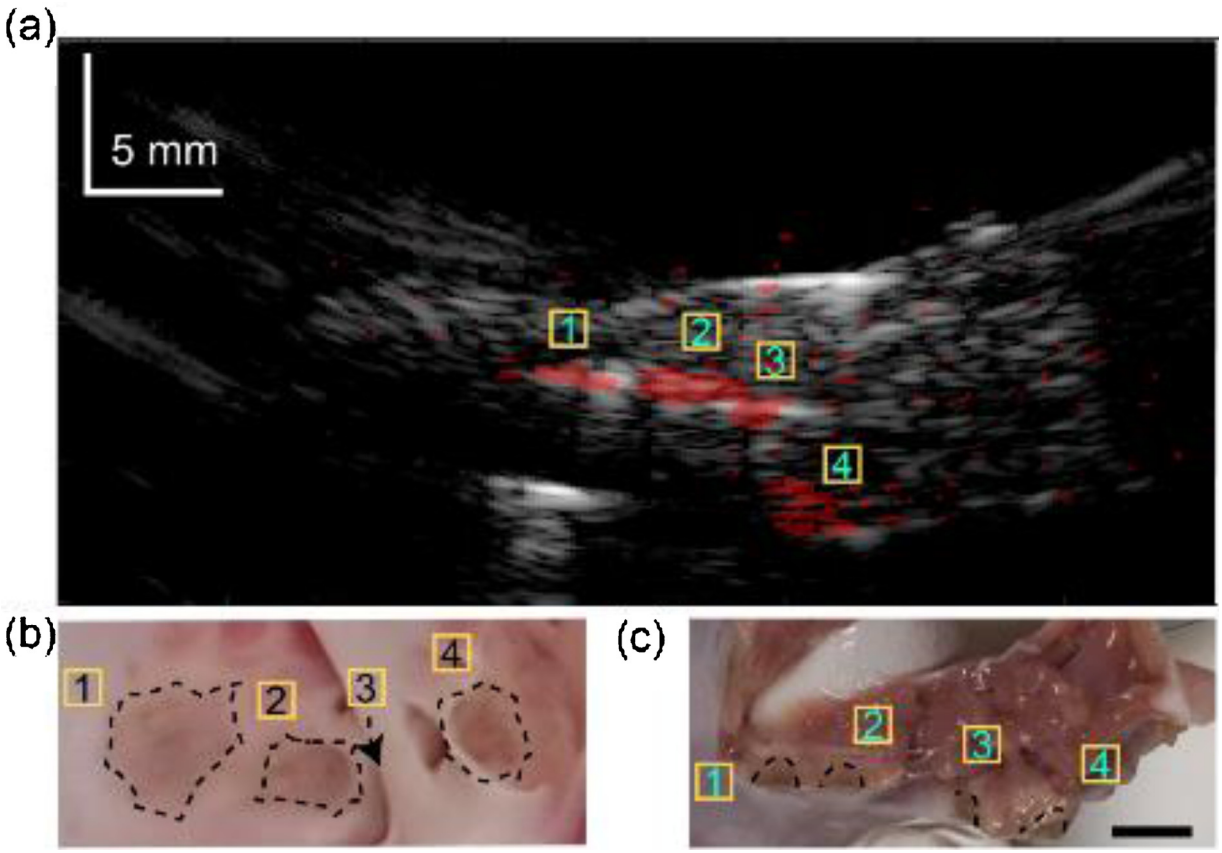

Fig. 3. Evaluation of lesion continuity. (a) Compound 2λPAI image. (b) Top view (endocardial side) of tissue; lesions 2 and 3 are continuous as visible in (a); 1 and 4 are separated from their respective adjacent lesions. Lesion 3 is inside the separate bundle structure as seen in (c). (c) Cross-section through the lesions (unfolding the tissue disconnected lesions 2 from 3). Scale bar represents 5 mm.

performance by changing the beating heart circulation medium to (deoxygenated) blood and monitoring the creation of another lesion. PA signals from tissue were successfully generated (Fig. 7b). Since both I_{790} and I_{930} displayed sufficient tissue SNR, we generated 2λPA images, and established that the imaging site was initially free from lesions (Fig. 7a, left panel). This confirms that blood does not generate false-positive lesion sites in 2λPA imaging. After the ablation, a clear signal indicating lesion presence is observed (Fig. 7a, right panel), and is corroborated with tissue examination (Fig. 7c). We have measured a lesion size of 3.6 × 2 mm (lateral x axial) after tissue examination, while the photoacoustic image showed a lesion size of 3.9 × 3 mm (lateral x axial). Lesions are growing in 3 dimensions and thus the lesion sizing is highly dependent on the matching between sectioned and imaged planes which was difficult in this highly mobile experiment. Movie 5 documents the ablation process (30 W, 60 s) through blood around the mitral valve annulus; the valve motion appears erratic due to the low imaging frame rate. Fig. 7d illustrates catheter positions, deduced from ICE image features. Acquisition in blood was performed with the three-fiber RFPA catheter after failure of the first prototype.

4. Discussion

4.1. Imaging system and method

Imaging of ablation lesion progression was achieved with dual-wavelength intracardiac photoacoustics, showing robust lesion contrast in the presence of blood and cardiac motion. Lesion formation, being a slow process (30–60 s), does not require a high frame rate for timely feedback. However, rapid acquisition between the two wavelengths constituting a 2λPA imaging frame is essential to ensure minimal sensitivity to motion and to guarantee that both $I_{\lambda 1}$ and $I_{\lambda 2}$ capture the same lesion stage. Averaging the S_R frames rather than the I_λ frames minimizes the occurrence of imaging glitches due to motion.

The non-negligible elevational focus of the imaging system, which varied with imaging depth, did not allow for an exact matching of images to cross-sectional tissue photographs. In future work, we will establish imaging resolution (e.g. minimum gap detection) and establish the PA contrast for different tissue ablative stages; these experiments require an improved lateral resolution and exact co-registration which can be obtained with a 3D scanning stage and a focused transducer. Following these considerations, we have also chosen not to perform a quantitative validation of lesion size comparing with histology. In previous experiments, we found that NTC (Nitro Blue Tetrazolium) stained sections provided the same information on ablation lesion location and extent as visual inspection. We verified whether lesions were continuous or not (maximum diameter) and transmural or not (maximum depth) based on visual inspection, documented in photographs.

2λPA images represent better the signal through depth than single wavelength I_λ images, which are saturated by the stronger signals from both the RFPA catheter metallic tip and tissue surface. A threshold value of $S_R > 1$ was used to robustly differentiate between the absence and presence of lesions in 2λPA images. Detected lesion signals were persistent, which means they originate from tissue changes and not from elevated temperature. Future work may establish a correlation between gradation of ablation lesions and S_R, potentially allowing identification of, for instance, reversible lesions, steam build-up, edema, and charring. In the experiments performed here, occasional hematoma-like damage to the tissue due to catheter contact force was not identified as a lesion.

In-depth tissue illumination is key to generate 2λPA images reflecting correct lesion extent, and reduces the sensitivity to superficial

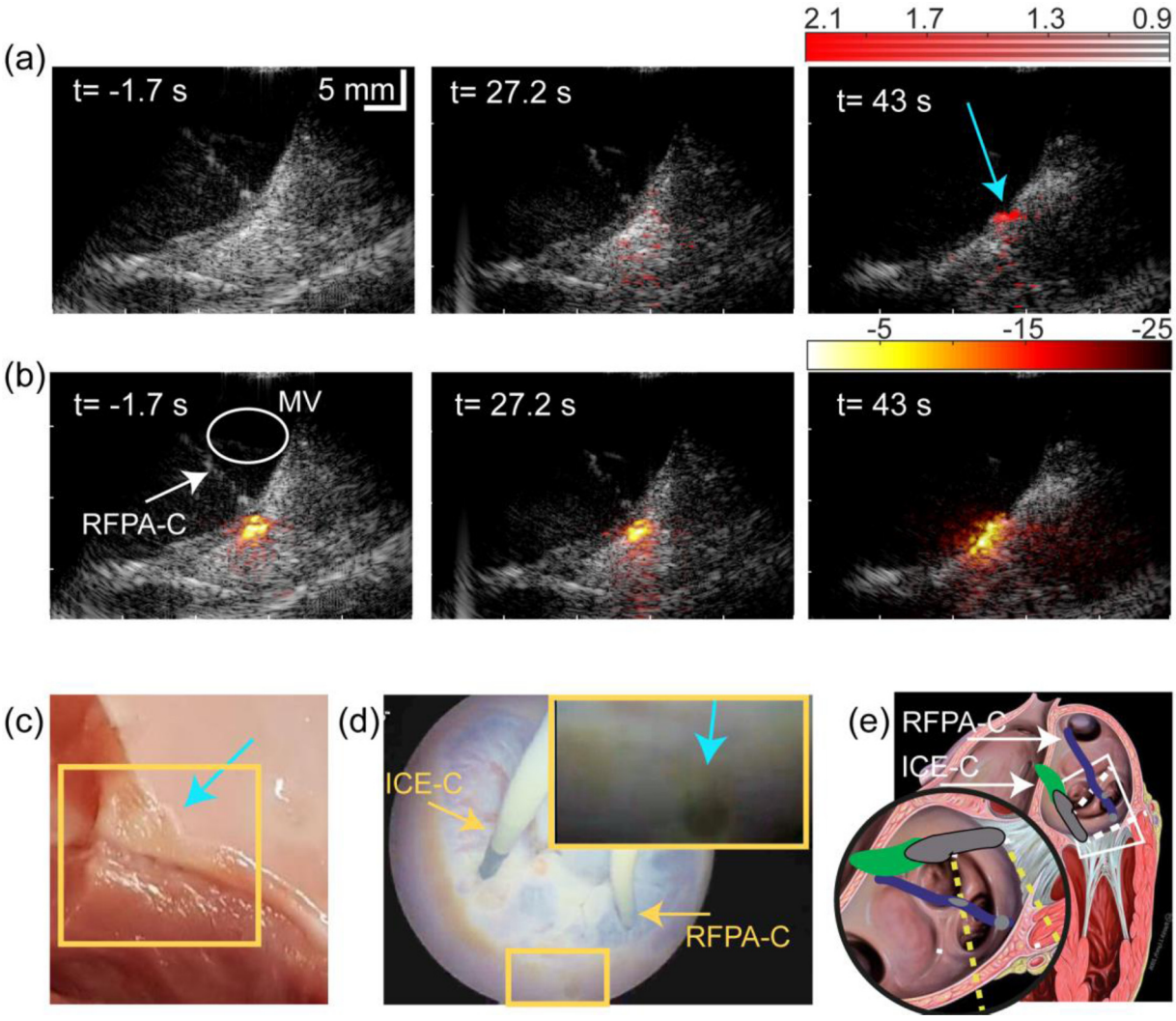

Fig. 4. Ablation monitoring in a beating heart. (a) 2λPA images before, during and after ablation, available as Movie 2. (b) I_{790} equivalents. 2λPA data confirm lesion formation. (c) Photograph of lesion made. (d) Video endoscopy frame confirming a lesion was made. (e) Sketch of instruments positions adapted from [31]. Round inset: ICE-C and RFPA-C relative to the valve, oriented as in the images in (a) and (b). ICE catheter (ICE-C); PA-enabled ablation catheter (RFPA-C). Mitral valve (MV). Cyan arrows indicate indentation formed by ablation.

(endocardium) optical properties. We fabricated two different prototypes of RFPA catheter. While we previously showed that these were performing equally, [27] we did not consider the factors of maneuverability and catheter orientation. A three-fiber prototype allowed for efficient tissue illumination for a larger set of ablation catheter contact angles than a single, centered fiber prototype. For instance, in Fig. 2, visualization of the lateral extent of the lesion is dependent on the orientation of the illumination; compound images obtained by moving the catheter were necessary to reveal the lateral extent of the lesion (Fig. 3). On ultrasound images, the RFPA catheter shaft echogenicity varied with the change in relative positions of the ICE and RFPA catheters due to cardiac motion. Fluctuations in both 2λPA images and I_{λ} signals may partially be related to catheter orientation and position within the ICE-C field of view; we notice that advancing or retracting

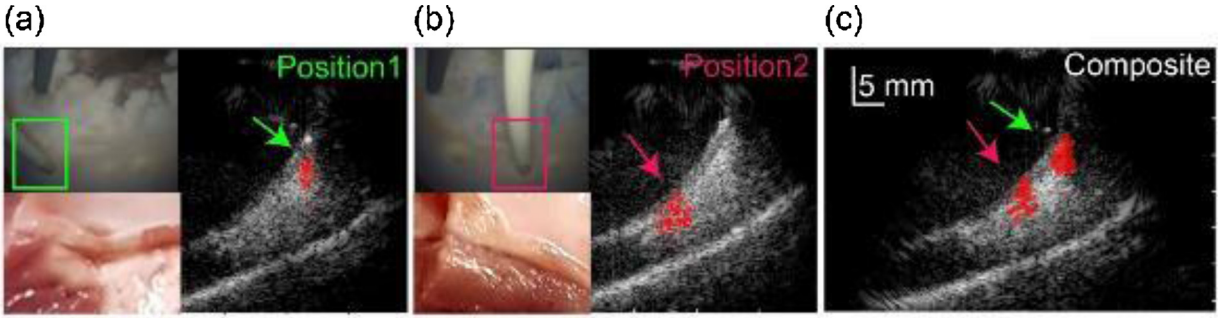

Fig. 5. Lesion continuity in a beating heart. 2λPA image, corresponding endoscope frames and lesions photographs of the newly formed lesion site (a); old lesion site (b) and the resulting composite image (c) available as Movie 3. Arrows indicate lesion sites.

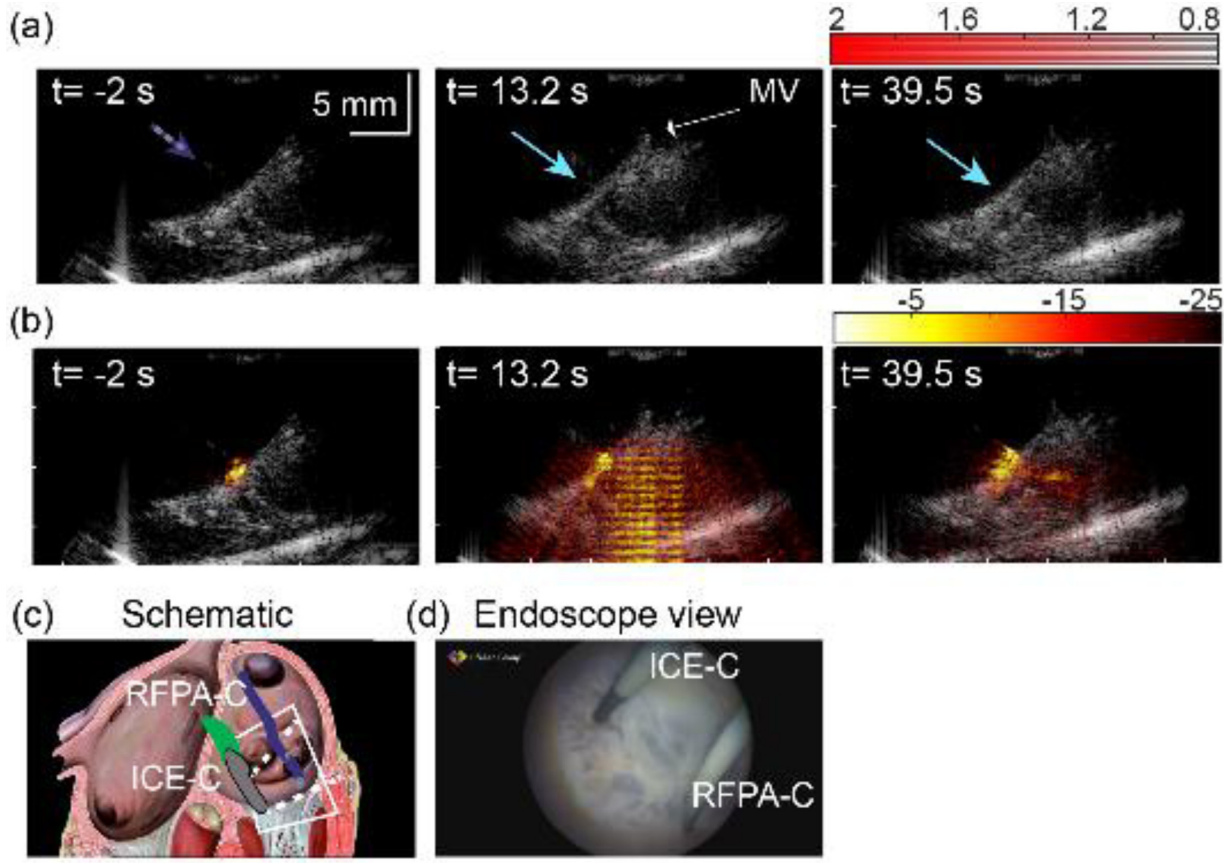

Fig. 6. True negative: monitoring of low-power RF energy delivery in a beating heart. (a) 2λPA images before, during and after energy delivery. (b). I790 equivalents. The 2λPA data confirm absence of lesion (Movie 4). Cyan arrows indicate the treated region. C. Sketch of instruments positions and imaging plane (adapted from [31]) as shown in (d). ICE-C: intracardiac echography catheter (green and grey); RFPA-C: PA-enabled ablation catheter (purple and grey); MV: mitral valve.

the catheter with respect to the tissue surface affects the collected signal. Effects of catheter design and catheter tip contact angle and force with tissue surface on signal generation shall thus be further studied.

4.2. Tissue handling and translation to in-vivo scenario

The results presented here, on fresh tissues (< 8 h from sacrifice in the intact hearts) partially perfused with deoxygenated blood, show that 2λPA imaging is not affected by the surrounding blood. However, 2λPA imaging is based on optical spectral contrast; live cardiac tissue perfusion and oxygenation will differ from our ex-vivo setup. Increased perfusion in vivo could affect the imaging depth and optical propagation paths due to blood scattering, but the well-characterized absorption spectra of blood and myocardium suggest that lesion contrast should be even stronger in a highly oxygenated scenario. Nevertheless, experimental validation is needed.

Some differences with clinical practice need to be addressed before generalization of the presented results. First, imaging was performed on a controlled, low heart rate, where in reality heartbeats can be fast and erratic during AF. Imaging artefacts due to motion and catheter orientation may thus be exacerbated in patients. A higher frame rate will certainly help in imaging more variable motion. Second, since the PV were tied together to prevent fluid outflow, we ablated around the mitral valve annulus. Since we did not see quantitative or qualitative differences between lesions produced in the static setup (which included atrial tissues near the PV) and in the beating heart, we assume that successful lesion monitoring and assessment on the mitral valve annulus is representative of imaging capability in other atrial locations. Third, we used porcine hearts, which are considered a representative model of the human heart, but our imaging results depend on detailed tissue optics and need to be confirmed on human atrial specimens. Preliminary experiments (Supplementary Fig. 1) as well literature studies [32] show that human and porcine cardiac tissues optical signature are similar in the wavelength range of interest. Our results are thus likely to be generalizable to human tissue ablation.

4.3. Clinical perspective

Unlike other proposed technology candidates to monitor RF ablation for AF, [13,15] 2λPA imaging allows both real-time monitoring and depth-resolved lesion continuity assessment. Our implementation builds on existing commercial technologies and requires minimal modification of current clinical routine, adding an unobtrusive layer of feedback on lesion quality during the procedure. Integration to current mapping systems could provide a 3D rendering of the PA-assessed lesion extent on the electroanatomical map. PA signals can be used to derive a number of useful parameters for intervention guidance beyond lesion quality: I_λ directly depends on tissue temperature; and signals from the catheter may assist navigation in atrial 3D-ICE volumes.

Future work targets in-vivo demonstration in animal models. Correlation of PA image characteristics to electrical lesion functionality, as well as to complications such as steam-pops, will define image interpretation for use in guidance of clinical interventions. Evaluation of the technology in a clinical research setting should demonstrate the practical value of PA imaging in ablative therapy of the atria. Gains in procedure safety, speed and efficacy are anticipated, but should be tested, and will precede any studies of impact on procedural success.

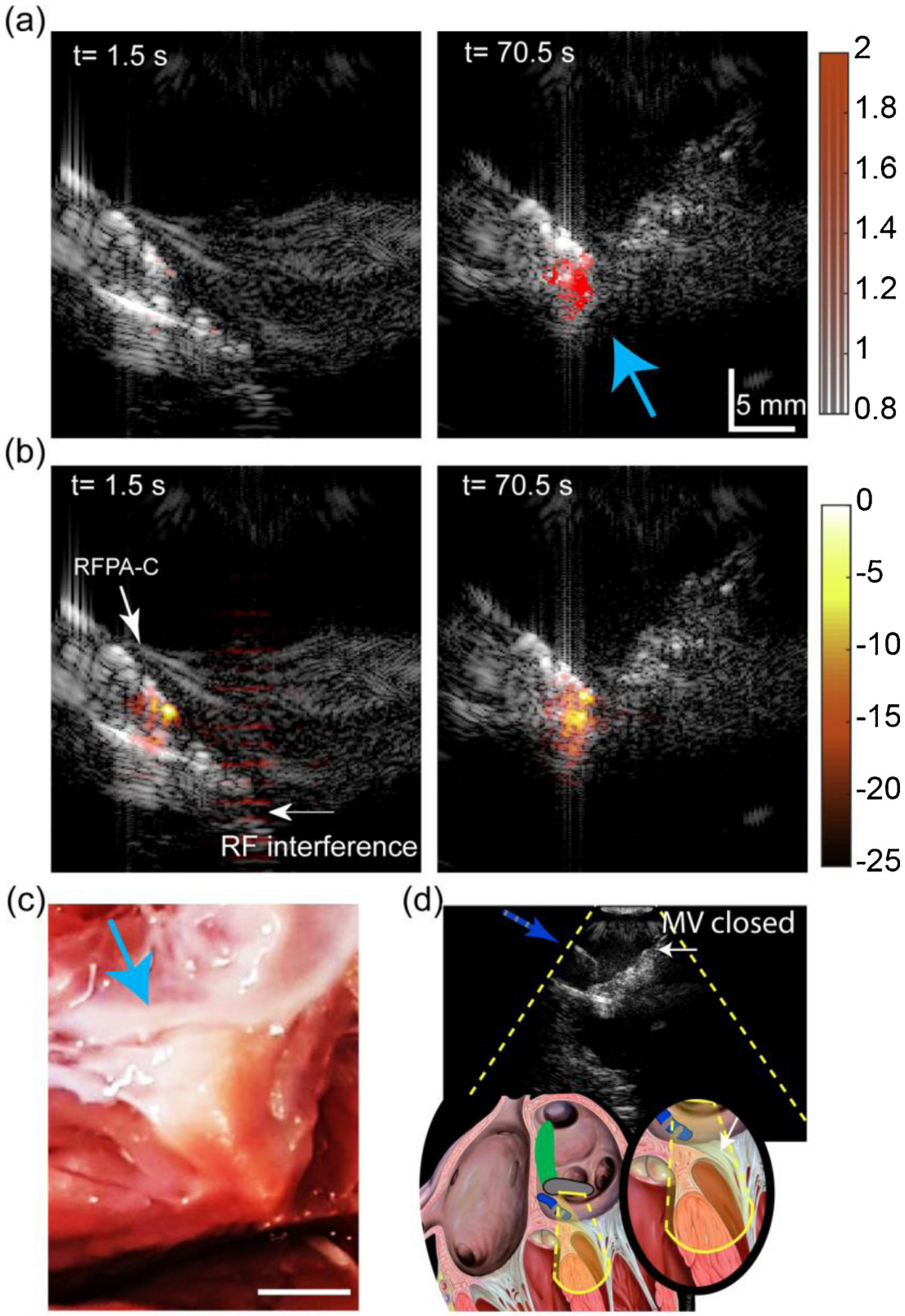

Fig. 7. Ablation monitoring in a beating heart filled with circulating blood. (a) 2λPA images at the beginning and after ablation and (b) I_{790} equivalents confirming presence of PA signal from tissue. (c) Photograph of the (superficial) lesion. (d) Sketch of instruments positions (adapted from [31]) Oval inset: ICE-C and RFPA-C relative to the valve, oriented as in the images in (a) and (b). (a) is available as Movie 5.

5. Conclusion

Dual wavelength photoacoustics (2λPA), based on the ratio of images acquired at 790 nm and 930 nm, can provide real-time monitoring of intra-atrial RF ablation procedures in a blood-filled beating heart. Videos of ablation lesion formation, and identification of lesion gaps were achieved, with clinically-translatable instruments, consisting of a modified ablation catheter for illumination and ICE for

signal detection. Using 2λPA signals from lesions could be discriminated from blood and healthy tissue, and were persistent after ablation. The presented solution has the advantage of being simple in implementation, easy to integrate and free from heuristics, modeling or time-consuming computations.

Funding

Netherlands Organisation for Scientific Research (NWO) (12706).

Declaration of Competing Interest

The authors have no conflicts to disclose

Acknowledgement

Martin Pekar, Hendrik J. Vos, Emile Peters, Lifetec team: Noemi Vanerio, Dave Wanders, Bart Smeets, Sjoerd van Tuijl.

Appendix A. Supplementary data

Supplementary material related to this article can be found, in the online version, at doi:https://doi.org/10.1016/j.pacs.2019.100150.

References

[1] S. Stewart, C.L. Hart, D.J. Hole, J.J.V. McMurray, A population-based study of the long-term risks associated with atrial fibrillation: 20-year follow-up of the Renfrew/Paisley study, Am. J. Med. 113 (5) (2002) 359–364.

[2] P. Kirchhof, S. Benussi, D. Kotecha, A. Ahlsson, D. Atar, B. Casadei, M. Castella, H.C. Diener, H. Heidbuchel, J. Hendriks, G. Hindricks, A.S. Manolis, J. Oldgren, B.A. Popescu, U. Schotten, B. Van Putte, P. Vardas, S. Agewall, J. Camm, G. Baron Esquivias, W. Budts, S. Carerj, F. Casselman, A. Coca, R. De Caterina, S. Deftereos, D. Dobrev, J.M. Ferro, G. Filippatos, D. Fitzsimons, B. Gorenek, M. Guenoun, S.H. Hohnloser, P. Kolh, G.Y. Lip, A. Manolis, J. McMurray, P. Ponikowski, R. Rosenhek, F. Ruschitzka, I. Savelieva, S. Sharma, P. Suwalski, J.L. Tamargo, C.J. Taylor, I.C. Van Gelder, A.A. Voors, S. Windecker, J.L. Zamorano, K. Zeppenfeld, 2016 ESC Guidelines for the management of atrial fibrillation developed in collaboration with EACTS, Eur. J. Cardio-thoracic Surg. 50 (5) (2016) e1–e88.

[3] N.F. Marrouche, J. Brachmann, D. Andresen, J. Siebels, L. Boersma, L. Jordaens, B. Merkely, E. Pokushalov, P. Sanders, J. Proff, H. Schunkert, H. Christ, J. Vogt, D. Bansch, C.-A. Investigators, Catheter ablation for atrial fibrillation with heart failure, N. Engl. J. Med. 378 (5) (2018) 417–427.

[4] E. Arbelo, J. Brugada, G. Hindricks, A.P. Maggioni, L. Tavazzi, P. Vardas, C. Laroche, F. Anselme, G. Inama, P. Jais, Z. Kalarus, J. Kautzner, T. Lewalter, G.H. Mairesse, J. Perez-Villacastin, S. Riahi, M. Taborsky, G. Theodorakis, S.A. Trines, A.F.A. Pil, The atrial fibrillation ablation pilot study: an european survey on methodology and results of catheter ablation for atrial fibrillation conducted by the european heart rhythm association, Eur. Heart J. 35 (22) (2014) 1466–U46.

[5] F.F. Ouyang, M. Antz, S. Ernst, H. Hachiya, H. Mavrakis, F.T. Deger, A. Schaumann, J. Chun, P. Falk, D. Hennig, X.P. Liu, D. Bansch, K.H. Kuck, Recovered pulmonary vein conduction as a dominant factor for recurrent atrial tachyarrhythmias after complete circular isolation of the pulmonary veins - Lessons from double lasso technique, Circulation 111 (2) (2005) 127–135.

[6] H. Calkins, K.H. Kuck, R. Cappato, J. Brugada, A.J. Camm, S.A. Chen, H.J.G. Crijns, R.J. Damiano, D.W. Davies, J. DiMarco, J. Edgerton, K. Ellenbogen, M.D. Ezekowitz, D.E. Haines, M. Haissaguerre, G. Hindricks, Y. Iesaka, W. Jackman, J. Jalife, P. Jais, J. Kalman, D. Keane, Y.H. Kim, P. Kirchhof, G. Klein, H. Kottkamp, K. Kumagai, B.D. Lindsay, M. Mansour, F.E. Marchlinski, P.M. McCarthy, J.L. Mont, F. Morady, K. Nademanee, H. Nakagawa, A. Natale, S. Nattel, D.L. Packer, C. Pappone, E. Prystowsky, A. Raviele, V. Reddy, J.N. Ruskin, R.J. Shemin, H.M. Tsao, D. Wilber, 2012 HRS/EHRA/ECAS expert consensus statement on catheter and surgical ablation of atrial fibrillation: recommendations for patient selection, procedural techniques, patient management and follow-up, definitions, endpoints, and research trial design, J. Interv. Card. Electrophysiol. 33 (2) (2012) 171–257.

[7] L. Ganjehei, M. Razavi, A. Rasekh, Catheter-based ablation of atrial fibrillation: a brief overview, Tex. Heart Inst. J. 38 (4) (2011) 361–363.

[8] K.H. Kuck, B.A. Hoffmann, S. Ernst, K. Wegscheider, A. Treszl, A. Metzner, L. Eckardt, T. Lewalter, G. Breithardt, S. Willems, G.-A.-A. Investigators, Impact of complete versus incomplete circumferential lines around the pulmonary veins during catheter ablation of paroxysmal atrial fibrillation results from the gap-atrial fibrillation-german atrial fibrillation competence network 1 trial, Circ-Arrhythmia Elec. 9 (1) (2016).

[9] F.H.M. Wittkampf, H. Nakagawa, RF catheter ablation: lessons on lesions, Pace 29 (11) (2006) 1285–1297.

[10] G. Rozen, L. Ptaszek, I. Zilberman, K. Cordaro, E.K. Heist, C. Beeckler, A. Altmann, Z. Ying, Z.J. Liu, J.N. Ruskin, A. Govari, M. Mansour, Prediction of radiofrequency ablation lesion formation using a novel temperature sensing technology incorporated in a force sensing catheter, Heart Rhythm 14 (2) (2017) 248–254.

[11] J. Inoue, A.C. Skanes, L.J. Gula, M. Drangova, Effect of left atrial wall thickness on radiofrequency ablation success, J. Cardiovasc. Electrophysiol. 27 (11) (2016) 1298–1303.

[12] E.J. Schmidt, H.R. Halperin, MRI use for atrial tissue characterization in arrhythmias and for EP procedure guidance, Int. J. Cardiovas. Imag. 34 (1) (2018) 81–95.

[13] J. Grondin, E. Wan, A. Gambhir, H. Garan, E.E. Konofagou, Intracardiac myocardial elastography in canines and humans in vivo, IEEE Trans. Ultrason. Ferroelectr. Freq. Control 62 (2) (2015) 337–349.

[14] M. Granier, P.F. Winum, M. Granier, P. Liaud, G. Cayla, P. Messner, J.-L. Pasquie, I. Schuster, Real-time atrial wall imaging during radiofrequency ablation in a porcine model, Heart Rhythm 12 (8) (2015) 1827–1835.

[15] M. Wright, E. Harks, S. Deladi, S. Fokkenrood, R. Brink, H. Belt, A.F. Kolen, D. Rankin, W. Stoffregen, D.A. Cockayne, J. Cefalu, D.E. Haines, Characteristics of radiofrequency catheter ablation lesion formation in real time in vivo using near field ultrasound imaging, JACC Clin. Electrophysiol. 4 (8) (2018) 1062–1072.

[16] J.F. Ren, F.E. Marchlinski, D.J. Callans, E.S. Zado, Lesion imaging characteristics associated with successful ablation of appropriate sinus tachycardia: an intracardiac echocardiographic study, J. Am. Coll. Cardiol. 37 (2) (2001) 128a-128a.

[17] S.H. Wong, G.C. Scott, S.M. Conolly, G. Narayan, D.H. Liang, Feasibility of noncontact intracardiac ultrasound ablation and Imaging catheter for treatment of atrial fibrillation, IEEE T Ultrason. Ferr. 53 (12) (2006) 2394–2405.

[18] R.P. Singh-Moon, C.C. Marboe, C.P. Hendon, Near-infrared spectroscopy integrated catheter for characterization of myocardial tissues: preliminary demonstrations to radiofrequency ablation therapy for atrial fibrillation, Biomed. Opt. Express 6 (7) (2015) 2494–2511.

[19] D.A. Gil, L.M. Swift, H. Asfour, N. Muselimyan, M.A. Mercader, N.A. Sarvazyan, Autofluorescence hyperspectral imaging of radiofrequency ablation lesions in porcine cardiac tissue, J. Biophotonics (2016).

[20] X.W. Zhao, X.Y. Fu, C. Blumenthal, Y.T. Wang, M.W. Jenkins, C. Snyder, M. Arruda, A.M. Rollins, Integrated RFA/PSOCT catheter for real-time guidance of cardiac radio-frequency ablation, Biomed. Opt. Express 9 (12) (2018) 6400–6411.

[21] D.M. Liang, D. Taeschler, C. Goepfert, P. Arnold, A. Zurbuchen, R. Sweda, T. Reichlin, H. Tanner, L. Roten, A. Haeberlin, Radiofrequency ablation lesion assessment using optical coherence tomography - a proof-of-concept study, J. Cardiovasc. Electrophysiol. 30 (6) (2019) 934–940.

[22] S.Y. Park, R.P. Singh-Moon, E.Y. Wan, C.P. Hendon, Towards real-time multispectral endoscopic imaging for cardiac lesion quality assessment, Biomed. Opt. Express 10 (6) (2019) 2829–2846.

[23] S.Y. Park, R.P. Singh-Moon, C.P. Hendon, Towards multispectral endoscopic imaging for cardiac lesion assessment and classification for cardiac ablation therapy, Diagnostic and Therapeutic Applications of Light in Cardiology 2018 (10471) (2018).

[24] G.A. Pang, E. Bay, X.L. Dean-Ben, D. Razansky, Three-dimensional optoacoustic monitoring of lesion formation in real time during radiofrequency catheter ablation, J. Cardiovasc. Electrophysiol. 26 (3) (2015) 339–345.

[25] S. Iskander-Rizk, P. Kruizinga, A.F.W. van der Steen, G. van Soest, Spectroscopic photoacoustic imaging of radiofrequency ablation in the left atrium, Biomed. Opt. Express 9 (3) (2018) 1309–1322.

[26] N. Dana, L. Di Biase, A. Natale, S. Emelianov, R. Bouchard, In vitro photoacoustic visualization of myocardial ablation lesions, Heart Rhythm 11 (1) (2014) 150–157.

[27] S. Iskander-Rizk, G. Springeling, P. Kruizinga, R.H.S.H. Beurskens, A.F.W. van der Steen, G. van Soest, Photoacoustic-enabled RF ablation catheters for lesion monitoring, 2018, IEEE International Ultrasonics Symposium (Ius) (2018).

[28] J. Rebling, F.J. Oyaga Landa, X.L. Dean-Ben, A. Douplik, D. Razansky, Integrated catheter for simultaneous radio frequency ablation and optoacoustic monitoring of lesion progression, Opt. Lett. 43 (8) (2018) 1886–1889.

[29] Y.S. Hsiao, X. Wang, C.X. Deng, Dual-wavelength photoacoustic technique for monitoring tissue status during thermal treatments, J. Biomed. Opt. 18 (6) (2013) 067003.

[30] A.M. Leopaldi, K. Wrobel, G. Speziali, S. van Tuijl, A. Drasutiene, W.R. Chitwood, The dynamic cardiac biosimulator: a method for training physicians in beating-heart mitral valve repair procedures, J Thorac. Cardiov. Sur. 155 (1) (2018) 147–155.

[31] P.J. Lynch, Medical illustrations by Patrick Lynch, 1987-2000. https://commons.wikimedia.org/wiki/Category:Medical_illustrations_by_Patrick_Lynch. (Accessed September 2018 2018).

[32] R.P. Singh-Moon, C.C. Marboe, C.P. Hendon, Near-infrared spectroscopy integrated catheter for characterization of myocardial tissues: preliminary demonstrations to radiofrequency ablation therapy for atrial fibrillation, Biomed. Opt. Express 6 (7) (2015) 2494–2511.

Sophinese Iskander-Rizk obtained the degree of electronics engineering at the American University in Cairo in 2011 and then joined Delft University of Technology to pursue a master's degree in biomedical engineering. She then joined in 2014 the biomedical engineering department at Erasmus MC, university medical center in Rotterdam to pursue a doctoral degree on biomedical imaging. Her research topic is photoacoustic imaging for cardiovascular application. Her interests span from robotics, wearable technology to medical imaging.

Pieter Kruizinga started his career on photoacoustic imaging at the lab of Prof. Stanislav Emelianov, University of Texas at Austin, USA and continued this work for his PhD research at the Erasmus MC, The Netherlands with Dr. Gijs van Soest and Prof. Ton van der Steen. His postdoctoral research shifted focus towards ultrasound imaging where he developed techniques for computational ultrasound and functional ultrasound imaging. With help of a large multi-million investment grant he recently co-founded CUBE - Centre of Ultrasound Brain imaging at Erasmus MC. This new centre aims to combine imaging science, neuroscience and neurosurgery to better understand the brain and brain diseases. Pieter Kruizinga is currently an assistant professor at the department of neuroscience at the Erasmus MC.

Robert Beurskens (1972), obtained his BSc. in Electrical Engineering in 1997 at the Fontys Hogeschool Venlo (NL). He then started working at Hauzer Techno Coating in Venlo (NL) as an electrical engineer working on industrial scale physical vapour deposition (PVD) equipment. In 1999 he started to work at the Prins Maurits Laboratorium in Rijswijk (NL) a branch of the Dutch organization for applied physics TNO. His main interest was the design, construction and operation of high voltage pulsed power systems for all kinds of civil and defense applications varying from foodstuff sterilization, atmospheric plasma's to electric reactive armor and counter measures. Since 2007 he works for the department of Biomedical Engineering at the ErasmusMC in Rotterdam (NL) as electronic designer and instrumentation technician. The main interests here are analogue and high frequency electronics for ultrasound applications.

Geert Springeling received a B.Eng degree in mechanical engineering from the Hogeschool Utrecht in 2010. Since 2005, he has been working at the Department EMI, Erasmus MC, Rotterdam. He worked on intravascular ultrasound, intravascular photoacoustic and OCT catheter development. His interests are precision engineering, micro mechanics and (fiber)-optics.

Frits Mastik received a BSc degree in Numerical Mathematics from the Dutch Mathematical Society in 1979. Since 1986 he is working in the department of Biomedical Engineering of the Thorax Center, Erasmus MC, Rotterdam. He worked on ultrasound tissue characterization, intravascular ultrasound and recently on high framerate imaging. In intravascular ultrasound he has worked on IVUS flow and on IVUS palpography. His work ranges from instrumentation to developing processing software to clinical studies. His interests are signal processing and visualization methods.

Natasja MS de Groot is cardiologist-electrophysiologist at the Erasmus Medical Center in Rotterdam. The title of her thesis was 'Mapping and Ablation of Atrial TachyArrhythmias; from Signal to Substrate'. At present, she is director of the unit translational electrophysiology and principal investigator of the Medical Delta Cardiac Arrhythmia Lab, a collaboration between the Technical University Delft and the Erasmus MC. Her expertise is on cardiac mapping, pathophysiology of atrial fibrillation and arrhythmias in patients with congenital heart disease.

Paul Knops (1975) studied Applied Physics at the Rotterdam University. After an internship in the Daniel den Hoed Cancer Center (*Dose Mapping of Electromagnetic Field Radiation during Hyperthermic Treatment of Superficial Tumors*), he obtained a BSc degree based on a thesis *"Development of High Pressure Shock Wave Gauge for Measurements in the Vincinity of the Explosion Point"* at TNO - Prins Maurits Laboratory. He started working at the Erasmus MC - Clinical Electrophysiology department and specialized in cardiac arrhythmias (IBHRE, EHRA). He joined the Translational Electrophysiology research group, which focuses on the mechanisms underlying atrial fibrillation. Today, he is involved in the clinical and experimental intra-operative high-resolution cardiac mapping program and the development of dedicated mapping electrode arrays.

Ton van der Steen (1964) is the head of Biomedical Engineering of the Thorax center, Erasmus MC. He is co-founder of the Medical Delta. He is professor in Biomedical Engineering at the Erasmus MC and professor in Applied Physics at the TU Delft. He is also Medical Delta professor and honorary visiting professor with the Chinese Academy of Sciences. His main scientific interest is in creating imaging modalities for the cardiovascular system. His main policy interest is generating technical solutions for sustainable health care. He is 2000 NWO PIONIER and 2007 Simon Stevin Master. He is a member of both the Netherlands Academy of Technology and Innovation and the Royal Academy of Arts and Sciences. He is Fellow of IEEE and the European Society of Cardiology. Since 2018 he is Chairman of the Medical Delta.

Gijs van Soest is an Associate Professor at the Thorax Center of the Erasmus MC in Rotterdam, the Netherlands. He leads the research group in invasive imaging, which focuses on new technology for imaging guidance for cardiovascular and other interventions. Trained as an experimental physicist (PhD 2001 University of Amsterdam, MSc 1997 University of Groningen) and specialized in optics and wave scattering, he is an expert on imaging and spectroscopy of cardiovascular pathology and therapy. He uses photoacoustic imaging, optical coherence tomography and ultrasonic imaging to study these phenomena.